Singular Points Location Pattern Analysis Based on Modes Interference

Jian Li[1,2], Ze-Xi Wang[1], Rong Li[1], Guang-Jie Han[1], Jun-Hao Li[3]*

[1] College of Information Science and Engineering, Hohai University, China
[2] Science and Technology on Underwater Vehicle Technogogy Laboratory, Harbin Engineering University, China
[3] College of Cryptography, Zhengzhou Information Engineering University, China
jian263@sina.com, 201320010020@hhu.edu.cn, 221320010006@hhu.edu.cn,
hanguangjie@gmail.com, 1720754765@qq.com

Abstract

Given the lack of research on the regularity of distribution of singular points, the singular points under different influence factors are analyzed. The location of singular points for adjacent modes group (AMG) generated by the interference modes is derived using normal modes theory in the far field of the ideal shallow waveguide. The singular points are verified by simulation, which compares the distribution of the acoustic field and singular points. Moreover, it is concluded that the number and distribution of singular points in the period of the interference structure of the field (PISF) has a relationship with order (lower order of AMG) and adjacent order (difference between two orders of AMG). The arrangement of upper-lower-two-points increases by 2 with each increase of order and is distributed at both ends of PISF. The arrangement of rhombic-four-points increases by 1 with each increase of adjacent order and increases alternately at both ends of PISF. Meanwhile, there is a periodic relationship between the depth of the source and the location of singular points.

Keywords: Interference modes, Singular points, Ideal shallow waveguide, Period of the interference structure of the field

1 Introduction

Since the 20th century, ocean exploration has been an important field of research worldwide, and the study of singular points is also significant. Interference modes generate singular points, which occur in environments with field properties.

Singular points were first discovered in 1985 and are distributed near the energy streamlines. Singular points are divided into vortex points and saddle points, which are the isolated extreme values of the corresponding flow function. The acoustic pressure (P) at the vortex point is close to 0 Pa, the average particle velocity ($|\overline{V}|$) at the saddle point close to 0 m/s, and the saddle points may also appear when the difference between P and $|\overline{V}|$ is an odd multiple of $\pi/2$ [1-2]. For the type judgment of singular points, it can be judged by the Jacobian of the average power flow density vector (J_R and J_z) of the periodic signal concerning the distance and depth of the waveguide. When the Jacobian is less than 0, it is a vortex point. Otherwise, it is a saddle point, and the power flux density vector around the vortex point is also divided into clockwise and counterclockwise; if the curl of the acoustic intensity vector $curl\ \mathbf{I} > 0$, the acoustic intensity is counterclockwise; otherwise, it is clockwise. The above is the description of the fundamental properties of singular points. Meanwhile, the combined receivers have developed, which provides a channel for the actual monitoring of singular points [3-4].

The singular points generated by interference modes under an ideal shallow waveguide are studied in [5]. Still, only the source is located on the bottom of the waveguide; the same goes for research on other waveguides [6]. In the presence of noise, the distribution of singular points is also related to the signal-to-noise ratio, and it is expected that the information of the waveguide can be obtained from the singular points [7]. Of course, the study of singular points is also far-reaching in electromagnetism [8-9].

The location of the singular points when the source is located at the bottom of the waveguide is mainly derived in [5], which ignores the influence of the depth of the source on the singular points. Therefore, to better study the relationship between singular points and source depth, the location formula of singular points is derived for the first time when the depth of the source is not fixed in this work, taking the source depth as the primary input parameter, and using MATLAB to write the simulation function. Two groups of singular points need to be analyzed if the source is located at the bottom of the waveguide [5, 10]. However, after adding more depth information about the source, the third group of singular points is found in this work.

2 Analysis of Waveguide Mode

The waveguide theory used in this paper is the normal modes, in the process of modeling the acoustic field of an ideal waveguide using the normal modes, the general solution of the vertical component, namely the eigenfunction, can be obtained. Different order eigenfunctions correspond to different mode functions, and different mode functions

*Corresponding Author: Jian Li; E-mail: jian263@sina.com
DOI: 10.53106/160792642023092405007

correspond to different nomal modes. Because the singular points is generated by modes interference, the mode analysis is necessary.

Pekeris waveguide with depth of 150 m is set, and a 50 Hz source is placed on the bottom of waveguide. Set the corresponding environment configuration file in the AT toolbox. MOD file contains the eigenvalue and mode distribution data of different mode functions. Read the file to obtain the corresponding waveguide mode excitation results, as shown in Figure 1 (using a constant sound velocity profile, with a constant sound velocity of 1500 m/s.).

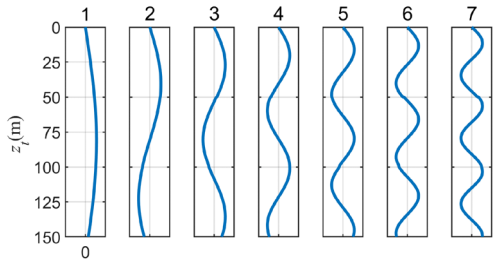

Figure 1. Mode results excited by 50 Hz source

The distribution of waveguide modes is mainly related to the sound speed profile, so add the sound speed profile shown in Figure 2 to the waveguide independent of distance (z_t is the true depth of the source, and the zero point of the depth coordinate is at the surface of the waveguide).

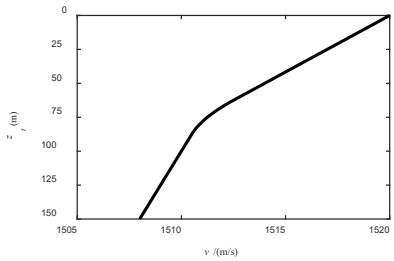

Figure 2. Negative gradient sound speed profile

The mode distribution after adding the profile is shown in the Figure 3. It can be seen that the mode peak of the first and second modes have shifted downward. Through further simulation, it can be found that the positive gradient sound speed profile will cause the mode peak to move up.

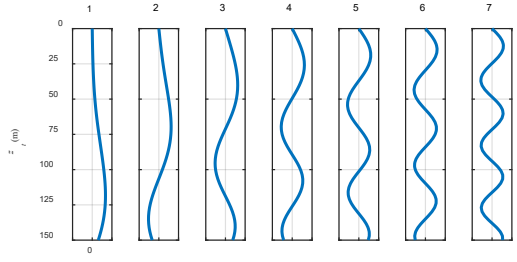

Figure 3. Modes distribution after adding negative gradient sound speed profile

3 Method of the Singular Points Location Acquisition

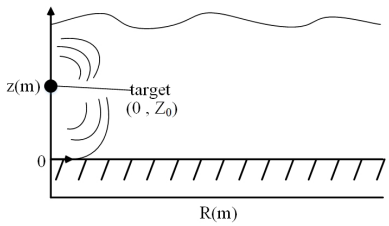

Figure 4. Simulation Environment Diagram (zero point of the depth coordinate is at the bottom of the waveguide)

Under the assumption of horizontal isotropy, the horizontal distance and the vertical depth are introduced to calculate the location of the singular points. The bottom value is the origin of vertical depth, which is presented in Figure 4. The top of the shallow waveguide is the vacuum. The bottom of the waveguide is elastic. When the location of the source is at $(0, Z_0)$, the acoustic field potential for large distances from the source is estimated by the following equation [5]

$$\Psi = -\frac{V_0}{4\pi} j \frac{2\pi}{H} \sqrt{\frac{2}{\pi R}} \exp(-j\frac{\pi}{4})\Omega, \tag{1}$$

$$\Omega = \sum_{m-l,q}^{m} \frac{1}{\sqrt{\xi_l}} \cos(b_l Z_0)\cos(b_l z)\exp[j(\xi_l R - \omega t], \tag{2}$$

Which V_0 is the strength of the source, H is the depth of waveguide, ξ_l and b_l are horizontal and vertical wave vectors of l -order mode respectively, ω is the circular frequency, $m = l$, q means l and q are the orders of the two interference modes, mode extraction can obtain the order of influence of the modes [11]. The waveguide acoustic pressure p and particle velocity V_R and V_z can be obtained by the acoustic field potential

$$p = -\rho\frac{\partial\Psi}{\partial t} \quad V_R = \frac{\partial\Psi}{\partial R} \quad V_z = \frac{\partial\Psi}{\partial z}. \tag{3}$$

The average power flow density vector in the horizontal and vertical directions over the signal period is as follows

$$\langle J_R \rangle = \frac{1}{2}\mathrm{Re}(pV_R^*) \quad \langle J_z \rangle = \frac{1}{2}\mathrm{Re}(pV_z^*), \tag{4}$$

Where * denotes complex conjugate, combine Equation (2) and (3), a system of equations related to z and R is obtained, where z and R represent the location of the singular points

$$\begin{aligned}\frac{R}{B}\langle J_R \rangle &= \cos^2(b_l Z_0)\cos^2(b_l z) + \cos^2(b_l Z_0)\cos^2(b_q z) \\ &+(2+\alpha)\cos(b_l Z_0)\cos(b_q Z_0)\cos(b_l z) \\ &\times\cos(b_q z)\cos\left[\left(\xi_l - \xi_q\right)R\right],\end{aligned} \tag{5}$$

$$\frac{R}{B}\langle J_z\rangle = [b_q\cos(b_l z)\sin(b_q z) - b_l\cos(b_q z)\sin(b_l z)] \times \frac{1}{\sqrt{\xi_l\xi_q}}\sin[(\xi_l-\xi_q)R]\cos(b_q Z_0]\cos(b_l Z_0), \quad (6)$$

Which satisfies $\alpha = (\xi_l+\xi_q)/(\sqrt{\xi_l\xi_q})-2$ and $B = \rho\omega V_0^2/(4\pi H^2)$ the location of the singular points can be determined when $< J_R > = < J_z > = 0$. The depth of the source is added as an essential parameter in obtaining the location of singular points, which was not covered in previous research.

3.1 Calculation of Location of First Group of Singular Points

By considering $\sin[(\xi_l - \xi_q)\ R] = 0$ in Equation (5), the result is

$$R = \frac{n\pi}{\xi_l - \xi_q}, \quad (7)$$

Which represents the horizontal distance of the first group of singular points; by substituting it into Equation (4), obtain

$$\frac{R}{B}\langle J_R\rangle = [\cos(b_l Z_0)\cos(b_l z) \pm \cos(b_q Z_0)\cos(b_q z)]^2 \pm\alpha\cos(b_l Z_0)\cos(b_q Z_0)\cos(b_l z)\cos(b_q z), \quad (8)$$

The value of α is minimal. To facilitate the calculation, the estimation idea is applied. By setting $\alpha = 0$ to get Equation (8) and Equation (9), the vertical estimated depths can obtain from (8) and (9).

$$\cos(b_l Z_0)\cos(b_l z') + \cos(b_q Z_0)\cos(b_q z') = 0, \quad (9)$$

$$\cos(b_l Z_0)\cos(b_l z') - \cos(b_q Z_0)\cos(b_q z') = 0, \quad (10)$$

z' is the vertical estimated depth of the first group of singular points, where Equation (8) and Equation (9) are the results of the setting $\cos[(\xi_l - \xi_q)\ R]$ in Equation (5) equal to +1 and -1, respectively. The actual depth of the first group of singular points is satisfied $\cos(b_l z) = \cos[b_l (z' + \Delta z)]$, by substituting it into Equation (7) to get the estimator Δz (the estimator is the difference between z' and z)

$$\Delta z \approx \frac{H\sqrt{\alpha}}{6\pi\tan(b_l z')\tan(b_l Z_0)}. \quad (11)$$

Further, obtain the first group of singular points' location as $(R, z' \pm \Delta z)$.

3.2 Calculation of Location of Second Group of Singular Points

By setting $b_q\cos(b_l z)\sin(b_q z) - b_l\cos(b_q z)\sin(b_l z) = 0$ in Equation (5), the vertical depth z is obtained and substituted into Equation (4), as well as the setting condition $\alpha = 0$, the horizontal estimated distance of the second group of singular points can be obtained

$$R' = \frac{\left[2\pi n + \arccos\left[\frac{\cos^2(b_l Z_0)+\cos^2(b_q Z_0)}{(2+\alpha)\cos(b_l Z_0)\cos(b_q Z_0)}\right]\right]}{\xi_l - \xi_q}, \quad (12)$$

R' satisfies $\cos((\xi_l - \xi_q)\ R')$ equals +1 or -1, which can correspond to the horizontal distance of the first group of singular points. Similarly, by putting R' into Equation (4), derive the estimator ΔR

$$\Delta R = \frac{\arccos\left[\frac{\cos^2(b_l Z_0)+\cos^2(b_q Z_0)}{(2+\alpha)\cos(b_l Z_0)\cos(b_q Z_0)}\right]}{\xi_l - \xi_q}. \quad (13)$$

Further, obtain the second group of singular points location as $(R' \pm \Delta R, z)$.

3.3 Calculation of Location of Third Group of Singular Points

By setting $\cos(b_q\ Z_0)\ \cos(b_l\ Z_0) = 0$ in Equation (5), the solutions of it are $Z_{0_1} = n\pi / 2b_q = nH / 2(q - 0.5)$ and $Z_{0_2} = n\pi / 2b_l = nH / 2(l - 0.5)$ respectively, substituting Z_{0_1} and Z_{0_2} into Equation (4), calculate the depth of the third group of singular points $z_1 = n\pi / 2b_l = nH / 2(l - 0.5)$ and $z_2 = n\pi / 2b_q = nH / 2(q - 0.5)$ respectively, z_1 and z_2 have nothing to do with R .

4 Simulation Verification of Singular Points

The waveguide normal waves determine the acoustic field at the receiver at large distances. The waveguide has multiple natural frequencies, and each natural frequency corresponds to the cut-off frequency of each order normal wave. When the source frequency more excellent than f_n [12], the corresponding n -order modes will be generated, the cut-off frequency of each mode function satisfies the following equation

$$f_n = \frac{(n-\frac{1}{2})c_1 c_2}{2H\sqrt{c_2^2 - c_1^2}}. \quad (14)$$

Where n is the maximum order of the mode excited by the source, c_1 and c_2 correspond to the sound speed of the waveguide medium and the sound speed of the seabed medium respectively. From the above equation, the equation of the modes order can be deduced

$$N < \frac{2f_n H\sqrt{c_2^2 - c_1^2}}{c_1 c_2} + \frac{1}{2}. \quad (15)$$

Table 1 and Table 2 are the modes number obtained by placing different frequency sources at the depth of 50 m in the Pekeris waveguide and changing the depth of the waveguide.

Table 1. Influence of source frequency on modes number when *sd* = 50m (*sd*: source depth)

Frequency (Hz)	Modes number
10	1
20	2
30	3
40	4
50	4
60	5
70	6
…	…
180	16

Table 2. Influence of waveguide depth on modes number when *sd* = 50m

Waveguide depth (m)	Modes number
22	1
44	2
66	3
75	3
88	4
100	4
110	5
…	…
200	9

Table 3. Simulation of shallow waveguide environment parameters

Parameters	Value
Source Frequency	50(Hz)
Source Depth	0-150(m)
Number of Media	1
Waveguide Depth	150(m)
Top Option	Vacuum
Bottom Option	Acoustic-Elastic
Number of Receiver Depths	150
Receiver Depths	0-150(m)
Sound speed -Waveguide	1500(m/s)
Sound speed -Bottom	2000(m/s)
Rho-Water	1(g/cm^3)
Rho-Bottom	2(g/cm^3)

The simulation of shallow ocean environment parameters is shown in Table 3. To better observe the distribution of the acoustic field in the two modes at a large distance, so plot the acoustic field of (1,7)-AMG under 20 periods of the interference structure of the field, set *sd* = 100m and *sd* = 150m respectively in Figure 5. The darker the color, the closer the value is to 0 Pa or 0 m/s. The acoustic pressure and particle velocity distributions of different depth sources exhibit a certain horizontal periodicity. For convenience, the singular points in 2 periods of the interference structure of the acoustic field will be analyzed after.

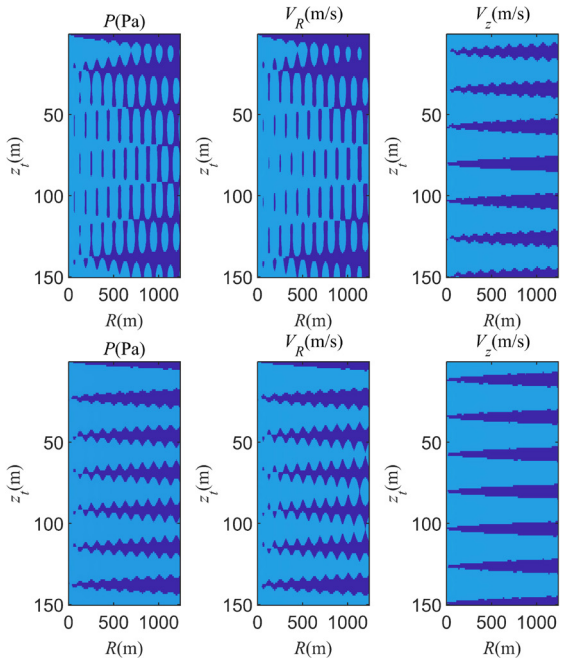

Figure 5. Acoustic pressure, particle velocity of (1,7)-AMG when *sd* = 100m and 150m (*sd*: source depth. The acoustic field simulation graphs are obtained through AT)

4.1 Verification of First and Second Group of Singular Points

Based on Table 3, set *sd* = 100m. Two AMGs (6,7) and (1,7) are chosen to simulate the acoustic field.

In the process of calculating the singular points position, because the calculation is too complex, the final singular points position can be obtained by graphical method, as shown in Figure 6 and Figure 7 for (6,7)-AMG (The red line in Figure 6 is obtained by substituting different z' into Equation (9), the black triangle on red line is the depth of the first group of singular points of $\cos((\xi_l - \xi_q)\, R') = 1$, the black line is obtained by substituting different z' into Equation (10), the red circle on the black line is the depth of the first group of singular points of $\cos((\xi_l - \xi_q)\, R') = -1$, the blue line in Figure 7 is obtained by substituting different z into $b_q \cos(b_l z) \sin(b_q z) - b_l \cos(b_q z) \sin(b_l z)$, and the red circle on the blue line is the depth of the second group of singular points. The corresponding depth coordinate in Figure are normalized.), Figure 8 and Figure 9 for (1,7)-AMG.

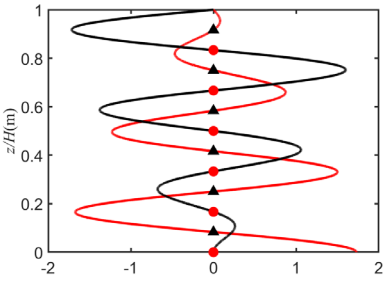

Figure 6. Depth coordinate analysis of the first group of singular points of (6,7)-AMG

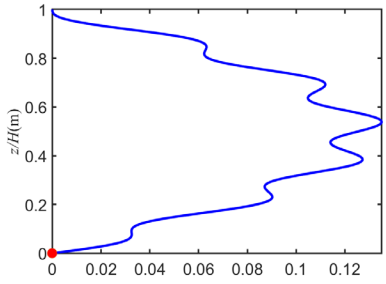

Figure 7. Depth coordinate analysis of the second group of singular points of (6,7)-AMG

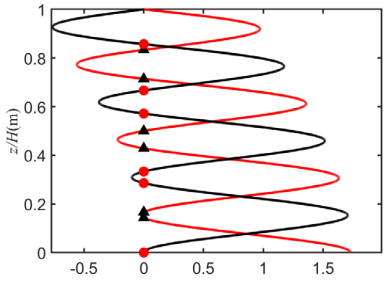

Figure 8. Depth coordinate analysis of the first group of singular points of (1,7)-AMG

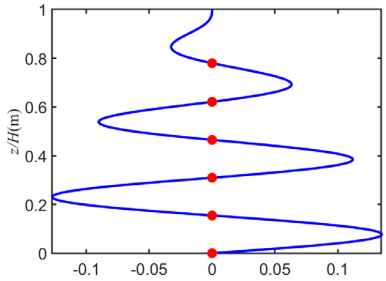

Figure 9. Depth coordinate analysis of the second group of singular points of (1,7)-AMG

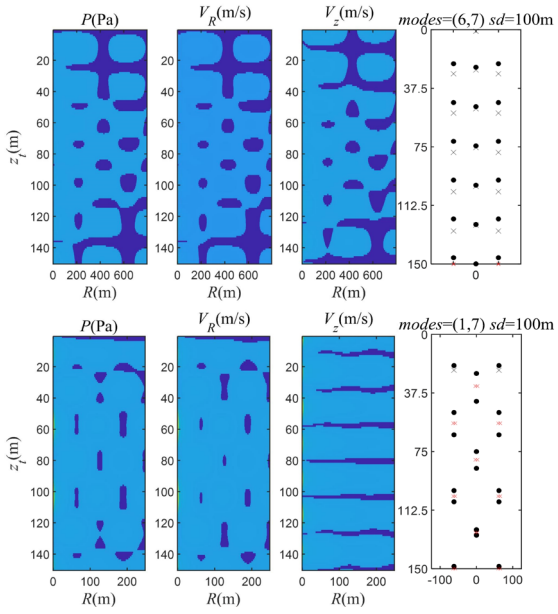

Figure 10. Comparison of acoustic pressure, particle velocity, and the singular points distribution of (6,7), (1,7) AMGs are corresponding to sd = 100m

The comparison of the acoustic pressure, particle velocity, and singular points distribution is presented in Figure 10 (the graph of the singular points is the implementation of the method of Section 2. There are only the first and second groups of singular points in the figure, ● is the vortex point, the black × is the first group of saddle points, and the red × is the second group of saddle points). It can be seen from Figure 10 that the acoustic pressure near-zero point and the particle velocity near-zero point of the AMG have a corresponding relationship with the distribution of the first two groups of singular points in location.

4.2 Verification of Third Group of Singular Points

The third group of singular points can be estimated using Equation (5). When $Z_{0_1} = n\pi / 2b_q = nH / 2(q - 0.5)$ and $Z_{0_2} = n\pi / 2b_l = nH / 2(l - 0.5)$, the depth of the third theoretical group of singular points are $z_1 = n\pi / 2b_l = nH / 2(l - 0.5)$ and $z_2 = n\pi / 2b_q = nH / 2(q - 0.5)$.

Considering that $l = 6$ and $q = 7$, which can get a third group of singular points with more. In this selected AMG, when the depth of the source satisfies $Z_t = 150 - 150n/\ 2\ (7 - 0.5) = 150 - 11.5385n$ (Z_t represents the actual depth of the source), there is the third group of singular points at a depth of (z_t means the true depth of the third group of singular points). Here, the case where $n = 1$ and $n = 2$ are shown in Figure 11 (the horizontal lines in the figure of singular points are the depth of the third group of singular points). As a result, the third group of singular points has nothing to do with source information, and there is no evidence from Figure 11 regarding their existence. So only the first and second group of singular points are analyzed in Section 5.

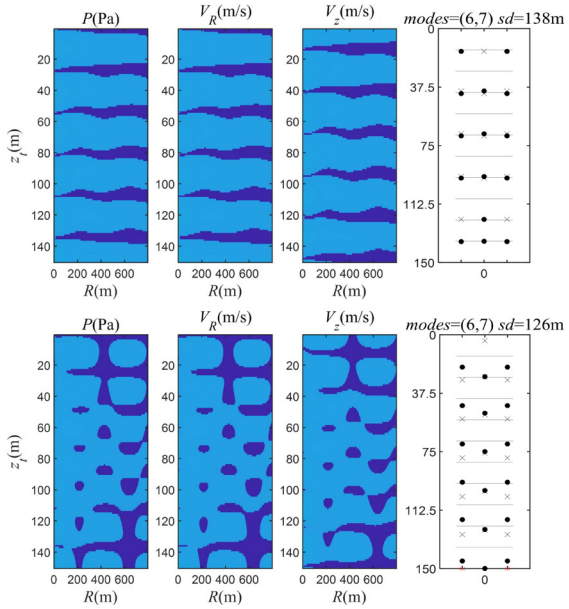

Figure 11. Comparison of acoustic pressure, particle velocity, and the singular points distribution of (6,7)-AMG corresponding to sd = 138m and 126m

5 Analysis of Singular Points for AMG

This Section analyzes singular points from three aspects: order, adjacent order, and source depth.

5.1 Analysis of Influence of Order on Singular Points

The source is placed on the seabed to investigate the effect, and the 1-AMG is analyzed. The source excites 1-7 modes, so six 1-AMGs are obtained, which are (1,2), (2,3), (3,4), (4,5), (5,6), and (6,7) AMGs. The distribution of the singular points of all 1-AMGs is shown in Figure 12. The condition $R = 0$ applies to the expression $R = \arccos(1)/(\xi_l - \xi_q)$, and the distance for the PISF corresponds to $R = \arccos(-1)/(\xi_l - \xi_q)$. It is clear from Figure 12 that the first group of singular points are distributed up and down. The order has an influence on the number (the number of groups of singular points) of singular points in 1 PISF: 1. The number of the first group of singular points is increased by a factor of 2 for each additional order; 2. The number of the first group of singular points is $num_x = 2 \times (x - 1)$, and x is the maximum order of 1-AMG.

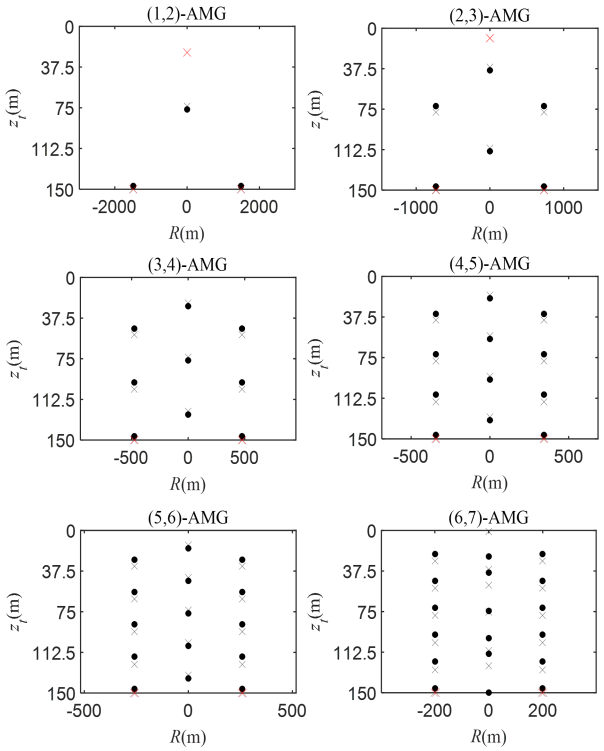

Figure 12. The distribution of the singular points of 1-AMG

To better analyze the number of the singular points, illustrate the numbers of all AMGs when $sd = 150$m and plot them as in Figure 13. As can be seen from Figure 13, the number of the first group of singular points for the lowest order n -AMG is $2n$, while all the numbers of the first group of singular points are increased by a factor of 2 by increasing the order, however, it has been verified this rule does not apply at all sd and is most pronounced at the surface, the center and the bottom of the waveguide. The number of the second group of singular points is $n + 1$, which decreases by a factor of 1 by increasing the order because the acoustic field disappears on the waveguide surface.

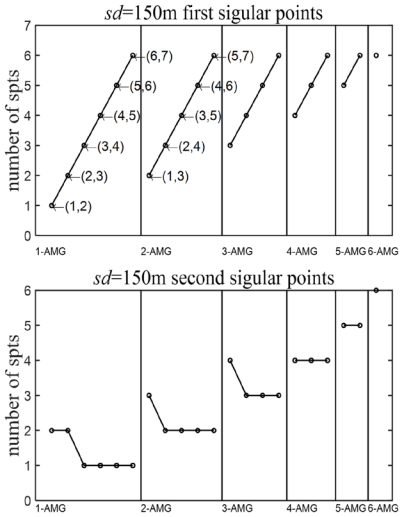

Figure 13. The number of the singular points of n -AMG corresponding to $sd = 150$m (The vertical depth is the number of the singular points for corresponding AMG, "spts" means singular points)

5.2 Analysis of Influence of Adjacent Order on Singular Points

To get a noticeable effect of the singular points distribution, the highest order AMGs are considered for analysis in this Section. The source is also placed on the seabed. The singular points distribution of (6,7), (5,7), (4,7), (3,7), (2,7), and (1,7) AMGs are illustrated in Figure 14.

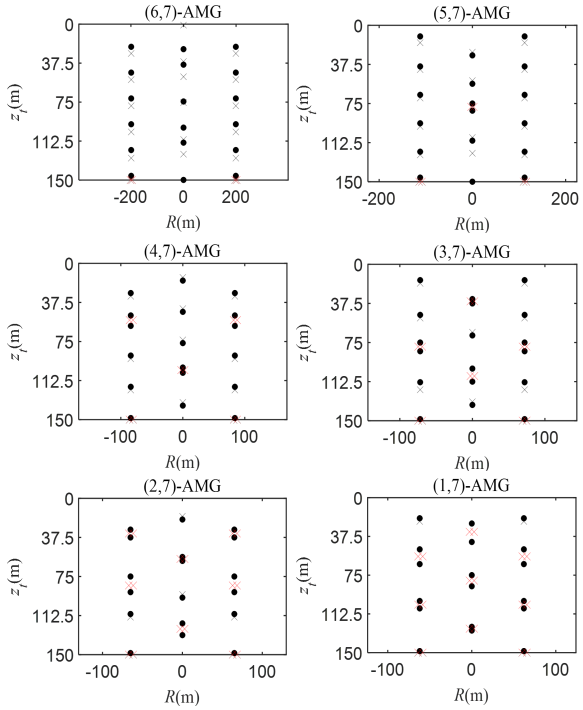

Figure 14. The singular points distribution of (6,7), (5,7), (4,7), (3,7), (2,7), (1,7) AMGs

It can be seen the rhombic-four-points arrangement starts to appear in 2-AMG. By increasing the adjacent order by a factor of 1, the rhombic-four-points arrangement increases alternately between R = arccos (1)/ ($\xi_l - \xi_q$) and R = arccos (−1)/ ($\xi_l - \xi_q$). Within one PISF, the number of rhombic-four-points arrangement corresponds to the n -AMG is n − 1. Moreover, the arrangement of the rhombic-four-points singular points appears from the center of the waveguide and gradually expands up and down. As a result, the distribution of the singular points of the highest adjacent order AMG is in the state of "upper-lower-two-points arrangement" up and "rhombic-four-points arrangement" down. The implementation of other n -AMGs follows the above conclusions.

5.3 Analysis of Influence of Sound Speed Profile on Singular Points

It can be seen from the Section 2 that the sound speed profile will affect the distribution of waveguide modes. Specifically, the influence of sound speed profile on waveguide modes can be analyzed from positive gradient, constant and negative gradient sound speed profiles. Three simple sound speed profiles are set by simulation such as Figure 15, Figure 16, and Figure 17.

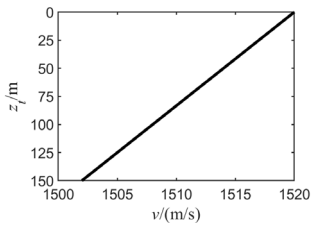

Figure 15. Negative gradient sound speed profile

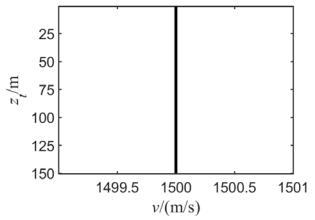

Figure 16. Constant sound speed profile

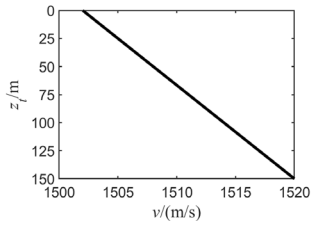

Figure 17. Positive gradient sound speed profile

The above three different sound speed profiles are added to the simulated waveguide in Table 3, and different modes distributions are obtained as shown in Figure 18, Figure 19, and Figure 20.

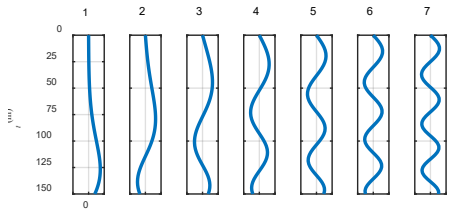

Figure 18. Modes distribution under negative gradient sound speed profile

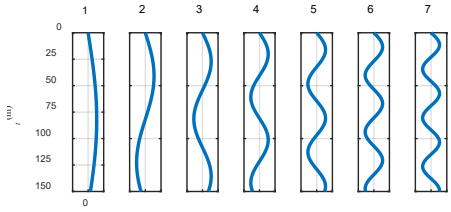

Figure 19. Modes distribution under constant sound speed profile

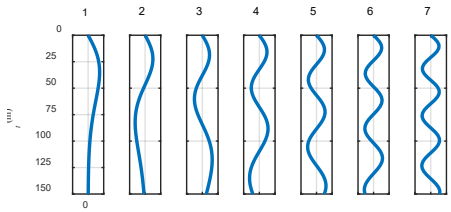

Figure 20. Modes distribution under positive gradient sound speed profile

It can be seen from the above figures that the influence of the sound speed profile on the low-order modes is relatively large, mainly concentrated in the first three modes; If the sound speed profile is a negative gradient profile, the mode peak will move downward as a whole; On the contrary, if the sound speed profile is a positive gradient profile, the mode peak will move up as a whole. Since the acoustic field singular points is generated by the interference between waveguide modes, the change of mode distribution will also lead to the change of the corresponding singular points distribution of AMG. In the process of deriving the formula for the location of the singular points, the wave number, the horizontal wave vector, and the PISF will be affected by the sound speed

$$k = \frac{2\pi f}{c}. \tag{16}$$

$$\xi_l = \sqrt{k^2 - b_l^2}. \tag{17}$$

$$R = \frac{\pi}{(\xi_l - \xi_q)}. \tag{18}$$

In Equation (16), c is the sound speed, and the sound speed corresponding to the sound speed profile, the sound speed of the non-constant sound speed profile will change with the depth, resulting in the wave number and the horizontal wave vector being affected by the change of the sound speed, thus leading to the change of the PISF. In order to better simulate and analyze, the first and second modes that are most affected by the sound speed profile are selected for simulation analysis. Place the source with a frequency of 50 Hz on the bottom of the waveguide, and the distribution of singular points obtained under different sound speed profiles is shown in Figure 21, Figure 22, and Figure 23.

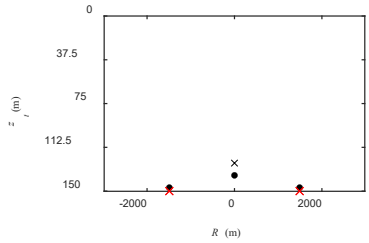

Figure 21. The distribution of singular points under negative gradient sound speed profile

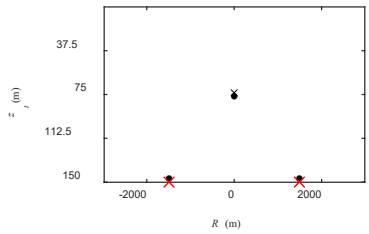

Figure 22. The distribution of singular points under constant sound speed profile

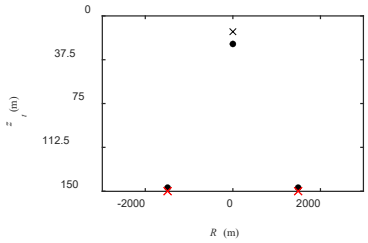

Figure 23. The distribution of singular points under positive gradient sound speed profile

It can be seen from the (1,2)-AMG singular points distribution figure that the negative gradient sound speed profile will cause the first and second order mode peaks to move down as a whole, and finally make the position of (1,2)-AMG singular points move down; The constant sound speed profile is a constant parameter in the ideal simulation environment. In this case, the mode peak is to the middle, which is the ideal mode distribution state, and the singular points is to the middle; The positive gradient sound speed profile will cause the first and second mode peaks to move up as a whole, and finally make the position of (1,2)-AMG singular points move up. If other AMG with many groups are selected for analysis, due to different sound speeds at different depths, not only speed displacement of singular points will occur, but also horizontal displacement will occur, and the analysis will be difficult.

5.4 Analysis of Influence of Source Depth on Singular Points

In order to better observe the effect of the change of source depth on the number of singular points, this section collects and analyzes the number of singular points corresponding to 1-AMG with many types of AMG. In order to simplify the analysis, only set the source depth as 10m to

Table 4. Number of singular points at different sound source depths (1-AMG)

	zt/m	(1,2)	(2,3)	(3,4)	(4,5)	(5,6)	(6,7)
The first group of singular points	10	2	4	6	8	10	12
	20	2	4	6	**6**	**8**	**10**
	30	2	4	**4**	**6**	10	12
	40	2	**2**	**4**	8	10	**10**
	50	2	**2**	6	8	**8**	12
	60	2	**2**	6	**6**	10	12
	70	2	4	6	**6**	10	**10**
	80	2	4	6	8	10	12
	90	**0**	4	**4**	8	10	**10**
	100	**0**	4	6	**6**	10	12
	110	2	4	6	8	**8**	12
	120	2	**2**	6	8	10	**10**
	130	2	4	**4**	8	10	12
	140	2	4	6	**6**	**8**	**10**
	150	2	4	6	8	10	12
	zt/m	(1,2)	(2,3)	(3,4)	(4,5)	(5,6)	(6,7)
The second group of singular points	10	2	2	1	1	1	1
	...	2	2	1	1	1	1
	150	2	2	1	1	1	1

150m with a spacing of 10m, and output the corresponding number of singular points by simulation. The results shown in Table 4 are obtained (the number of singular points is not consistent with the rule in Section 5.1 in bold).

It can be seen from the Table 4 that when the depth of the source changes, the number of the first group of singular points is not completely in accordance with Section 5.1 with $num_x = 2 \times (x - 1)$, which is only applicable to three special cases where the source is located at the surface, middle and bottom of the waveguide; The number of the second group of singular points is consistent with the rule described in Section 5.1. As the order of AMG increases, the sound pressure disappears on the waveguide surface, so the number of the second group of singular points will eventually decrease by one, and the rule will not change with the depth of the sound source.

To investigate the distribution of the singular points, it is essential to analyze the highest-adjacent-order AMG. Figure 24 depicts the distribution of the singular points of (1,7)-AMG when the source is placed at 25 m, 50 m, 75 m, 100 m, 125 m and 150 m respectively. Two conclusions can be ascertained from Figure 24.

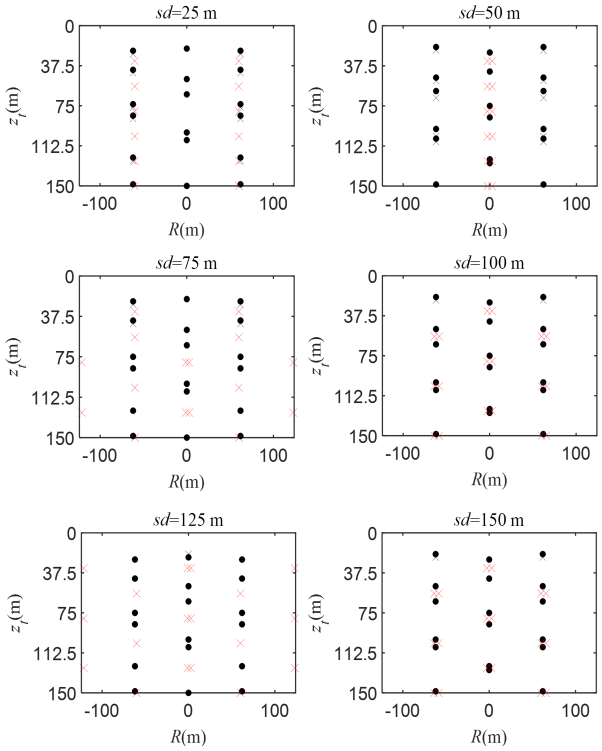

Figure 24. The distribution of the singular points corresponding to (1,7)-AMG varies with the source

- The depth of the first group of singular points varies periodically with the source's depth. Figure 25 illustrates the depth variation of the first group of singular points on the bottom of the waveguide corresponding to sources at different depths;
- The second group of singular points' estimator changes periodically with the source's depth, so the size of the estimator of the (1,7)-AMG obtained from different depths of the source is illustrated in Figure 26.

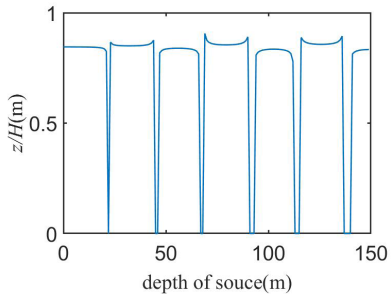

Figure 25. Variation of the depth of the first group of singular points with the source depth

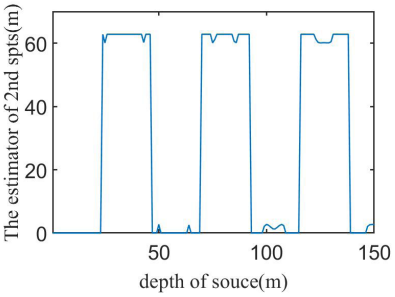

Figure 26. Variation of the estimator of the second group of singular points with the depth of the source

6 Conclusion

This work has analyzed the influencing factors and distribution regularity of interference modes singular points in the ideal shallow waveguide, the number and distribution of singular points are affected by many factors, including order and adjacent order. And under the premise of keeping other conditions unchanged, the distribution regularity of singular points of different source depths is analyzed; this part of the work can be used as the basis for the subsequent acquisition of source depth information through singular points, which can not only help the target data acquisition of underwater sensor networks [13-15] but also expand a new source depth acquisition idea.

Acknowledgment

Funding: This work is supported by the National key R&D Program (2022YFB4703403), the NSF of China (Grant No. 12274113), and in part by the Research Fund from Science and Technology on Underwater Vehicle Technology Laboratory (No. 6142215200102).

References

[1] C. F. Chien, R. V. Waterhouse, Singular points of intensity streamlines in two-dimensional sound fields, *The Journal of the Acoustical Society of America*, Vol. 101, No. 2, pp. 705-712, February, 1997.

[2] C. F. Chien, R. V. Waterhouse, Singular points of

intensity streamlines in axisymmetric sound fields, *Journal of Sound and Vibration*, Vol. 228, No. 4, pp. 931-937, December, 1999.
[3] E. G. Williams, Supersonic acoustic intensity, *The Journal of the Acoustical Society of America*, Vol. 97, No. 1, pp. 121-127, January, 1995.
[4] A. Zhukov, A. Ivannikov, V. Pavlov, Identification of multipole sound sources, *Soviet physices acoustics-ussr*, Vol. 36, No. 3, pp. 447-453, May-June, 1990.
[5] V. Eliseevnin, Y. I. Tuzhilkin, Acoustic power flux in a waveguide, *Acoustical Physics*, Vol. 47, No. 6, pp. 688-694, November, 2001.
[6] O. S. Chaika, M. O. Yaroshenko, O. V. Korzhyk, Singular points of vector intensity's field in waveguide with combine boundaries, *Mikrosistemi, Elektronika ta Akustika*, Vol. 23, No. 1, pp. 44-51, February, 2018.
[7] V. A. Shchurov, Peculiarities of real shallow sea waveguide vortex structure, *The Journal of the Acoustical Society of America*, Vol. 145, No. 1, pp. 525-530, January, 2019.
[8] I. Dzedolik, Singular points in the electromagnetic field-waveguide system, *Technical Physics Letters*, Vol. 29, No. 3, pp. 194-196, March, 2003.
[9] G. Makarov, V. Lobanov, Propagation of electromagnetic waves in a longitudinally inhomogeneous waveguide at the presence of singular points, *International journal of geomagnetism and aeronomy*, Vol. 6, No. 3, pp. GI3002 (1-7), August, 2006.
[10] Z. Wang, J. Li, Z. Zhang, M. Gu, Relationship between singular points of the acoustic field in the ideal shallow waveguide and source depth, *Journal of Applied Acoustics*, Vol. 42, No. 1, pp. 107-115, January, 2023.
[11] T. B. Neilsen, E. K. Westwood, Extraction of acoustic normal mode depth functions using vertical line array data, *The Journal of the Acoustical Society of America*, Vol. 111, No. 2, pp. 748-756, February, 2002.
[12] L. Brekhovskikh, Waves in layered media, *Elsevier*, 2012.
[13] G. Han, X. Long, C. Zhu, M. Guizani, Y. Bi, W. Zhang, An AUV Location Prediction-Based Data Collection Scheme for Underwater Wireless Sensor Networks, *IEEE Transactions on Vehicular Technology*, Vol. 68, No. 6, pp. 6037-6049, June, 2019.
[14] G. Han, X. Long, C. Zhu, M. Guizani, W. Zhang, A High-Availability Data Collection Scheme based on Multi-AUVs for Underwater Sensor Networks, *IEEE Transactions on Mobile Computing*, Vol. 19 No. 5, pp. 1010-1022, May, 2020.
[15] J. Li, M. Gu, T. Zhu, Z. Wang, Z. Zhang, G. Han, Research on Error Correction Technology in Underwater SINS/DVL Integrated Positioning and Navigation, *Sensors*, Vol. 23, No. 10, Article No. 4700, May, 2023.

Biographies

Jian Li, PhD, Associate Professor. College of Information Science and Engineering, Hohai University. Member of the China Acoustics Society, Jiangsu Ocean Society. Research interests include: underwater acoustic communication, detection, positioning and navigation, etc. Current projects: National Natural Science Foundation of China (NSFC), NSF of Jiangsu Province, National Key R&D Plan, etc.

Ze-Xi Wang received his bachelor's degree in Internet of Things Engineering from Hohai University in 2020. He is currently a master's student in the College of Information Science and Engineering at Hohai University. His research topics include applications in Underwater acoustic communication, computational ocean acoustics.

Rong Li received his bachelor's degree in Internet of Things Engineering from Hohai University in 2022. He is currently a master's student in the College of Information Science and Engineering at HoHai University. His research topics include waveguide singular points, underwater acoustics, IoT.

Guang-Jie Han is currently a Professor with the College of Information Science and Engineering, Hohai University, China. He is a Fellow of the UK Institution of Engineering and Technology. He has been awarded 2020 IEEE Systems Journal Annual Best Paper Award and the 2017-2019 IEEE ACCESS Outstanding Associate Editor Award.

Jun-Hao Li is a master of computer science in the School of Cryptography Engineering, Information Engineering University of Zhengzhou. During his school years, he participated in data mining and information security competitions and received corresponding awards.